ROCKY MOUNTAIN
JOURNAL OF MATHEMATICS
Volume 8, Numbers 1 and 2,
Winter and Spring 1978

CYLINDRICAL AND SPHERICAL SOLITONS

STEPHEN MAXON*

ABSTRACT. In this paper we review briefly the recent prediction and observation of cylindrical and spherical ion acoustic solitons in a cold, single species plasma. The properties of these higher dimensional solitons are quite different from their planar counterpart since the amplitude increases, the width decreases, and the propagation speed increases as the soliton moves inward.

Although the results for two- and three-dimensional solitons are obtained numerically, early time solutions can be found analytically and compared with numerical solutions. An interesting phenomenon, which is an integral part of these higher dimensional solitons, is the presence of a wake. Although the amplitude of this wake is very small, it can carry considerable momentum since it extends over a large spatial region.

1. **Introduction.** Planar soliton solutions for ion acoustic waves propagating in a collisionless plasma are well known (for a comprehensive review of the subject, see [1]). The initial value problem for the Korteweg-deVries (*KdV*) equation can be solved numerically, by the inverse method, or by using the conservation laws to find the asymptotic state of N solitons plus continuum. The experimental observation of N soliton breakup and the shape and speed preserving interaction of two solitons is well founded. We remind the reader that the planar soliton is a symmetric pulse moving with constant velocity, for which the square root of the amplitude multiplied by the width is a constant.

Considering the situation where the wave front is curved, and the propagation takes place radially, we expect quite different results. If a solution exists which has support only on a thin cylindrical or spherical shell, the amplitude will have to increase as the radius of the shell gets smaller, so that energy can be conserved. Since the amplitude, width, and propagation speed of soliton solutions are related to one another, we expect these quantities to change considerably as the wave proceeds inward or outward.

2. **Spherical Solitons [2].** We assume a collisionless plasma with isothermal electrons and cold ions. A disturbance occurs at some finite radius r_0. This causes a perturbation in the ion density N and the elec-

*Work performed under the auspices of the U.S. Energy Research and Development Administration under Contract No. W-7405-Eng-48.

Copyright © 1978 Rocky Mountain Mathematics Consortium

tron density n. The ions acquire a fluid velocity V and the charge separation causes an electric field E. The perturbation (n, N, V, E) then moves inward toward the singular point $r = 0$.

The fluid equations are

$$\frac{\partial V(r, t)}{\partial t} + V \frac{\partial V}{\partial r} = (Ze/M) E(r, t), \tag{1}$$

the momentum equation for the ion fluid,

$$\frac{\partial N(r, t)}{\partial t} + r^{-2} \frac{\partial}{\partial r} (r^2 NV) = 0, \tag{2}$$

the continuity equation for the ion fluid, and

$$\frac{\partial n(r, t)}{\partial r} = -(e/kT) En, \tag{3}$$

the equation for the stationary electron fluid. These are supplemented by Poisson's equation

$$r^{-2} \frac{\partial}{\partial r} (r^2 E) = 4\pi e(ZN - n). \tag{4}$$

Ze is the ion charge and T is the electron temperature. The electrostatic field E is in the r direction.

In order to obtain small amplitude solutions to the system (1)–(4), we follow the method of Washimi and Taniuti. The dispersion relation for acoustic waves [linearized solution to (1)–(4)], in the long wave length limit, leads to a choice of dimensionless co-ordinates

$$\xi = -\sqrt{\epsilon}(r/\lambda_D + \omega_i t) \tag{5}$$

and

$$\eta = \epsilon^{3/2} \omega_i t \tag{6}$$

where ϵ is the expansion parameter,

$$\lambda_D = \left(\frac{kT_e}{4\pi n_0 e^2} \right)^{1/2} \tag{7}$$

is the Debye length, and

$$\omega_i = \left(\frac{4\pi n_0 Z^2 e^2}{M} \right)^{1/2} \tag{8}$$

is the ion plasma frequency. The fluid quantities are expanded according to

$$n = n_0 + n' \tag{9}$$

and

$$N = (1/Z)(n_0 + N'), \tag{10}$$

where

$$n' = \epsilon n^{(1)} + \epsilon^2 n^{(2)} + \cdots, \tag{11}$$

$$N' = \epsilon N^{(1)} + \epsilon^2 N^{(2)} + \cdots, \tag{12}$$

$$V = \epsilon V^{(1)} + \epsilon^2 V^{(2)} + \cdots, \tag{13}$$

$$\tilde{E} = \epsilon \tilde{E}^{(1)} + \epsilon^2 \tilde{E}^{(2)} + \cdots, \tag{14}$$

and

$$E = \sqrt{\epsilon}\, \tilde{E}. \tag{15}$$

The first order equations give

$$n^{(1)} = N^{(1)} \tag{16}$$

$$\tilde{E}^{(1)} = \frac{(4\pi n_0 kT)^{1/2}}{c_s} \frac{\partial V^{(1)}}{\partial \xi} \tag{17}$$

and

$$n^{(1)} = -(n_0/c_s)V^{(1)} \tag{18}$$

where $c_s = (ZkT/M)^{1/2}$ is the sound speed.

The second order equations, together with equations (16)–(18), yield a modified *KdV* equation for the dimensionless first-order ion fluid velocity:

$$\frac{\partial U}{\partial \eta} + \frac{U}{\eta} + U \frac{\partial U}{\partial \xi} + \frac{1}{2} \frac{\partial^3 U}{\partial \xi^3} = 0 \tag{19}$$

where

$$U = -V^{(1)}/c_s. \tag{20}$$

Note that the *KdV* equation for spherical solitons has an additional term U/η compared to the equation for the planar case [1].

Equation (19) is a good approximation to the system (1)–(4) for weak dispersion $[(k\lambda_D)^2 = O(\epsilon)]$, weak nonlinearity $[\delta n/n_0 = O(\epsilon)]$, and large radius $[r/\lambda_D = O(\epsilon^{-3/2})]$. The condition on the radius comes from insisting that the solution which travels to the right along the ξ axis should not cross the $r = 0$ singularity, which travels to the left.

A solution was obtained by James Viecelli by numerically integrating (19) using an initial condition corresponding to a one-dimensional soliton,

$$U(\eta_0, \xi) = 3\,\mathrm{sech}^2(\xi/\sqrt{2}). \tag{21}$$

Without the U/η term in (19), the initial pulse would propagate to larger ξ values without changing its amplitude or shape, with a dimen-

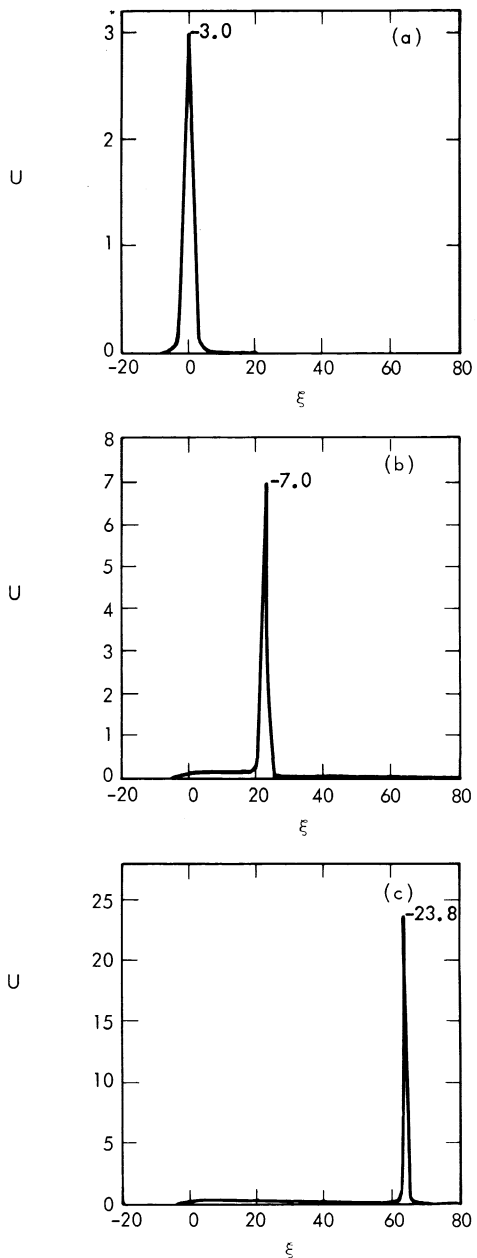

Figure 1. Evolution of spherical soliton. Dimensionless U versus spatial coordinate ξ at times (a) $\eta = -31.6$ (initial condition), (b) $\eta = -16.6$ and (c) $\eta = -6.6$.

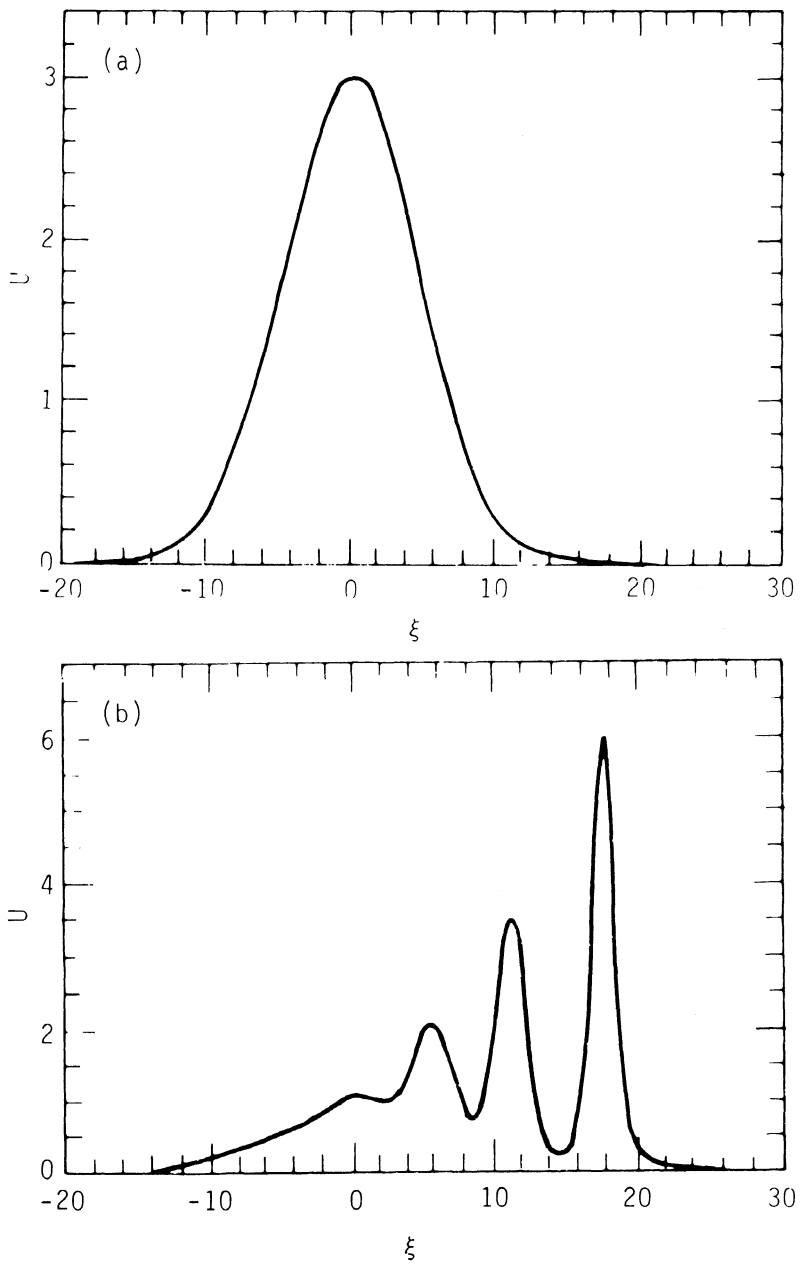

Figure 2. Breaking of radial disturbance into spherical solitons at (a) initial time and (b) later time.

sionless propagation velocity 1.0. With the U/η term present, our spherical soliton develops according to Figures 1(a)–1(c). As time increases and the solution propagates to larger ξ, the value of U increases, the width decreases, and a small residue is left behind the advancing pulse. In the lab frame, the pulse moves inward at an increasing speed somewhat greater than sound speed. It is found that the square root of the peak amplitude multiplied by the width (full width at half-maximum) of the pulse is constant to within 2% over the entire run $-31.6 \leqq \eta \leqq -6.6$.

An approximate solution to (19) for early times ($\eta \simeq \eta_0$) is

$$U^{(1)}(\eta, \xi) = U_0(\eta_0/\eta)\,\mathrm{sech}^2\{(U_0\eta_0/6\eta)^{1/2}[\xi - \xi_0 - 1/3\,\eta_0 U_0 \ln(\eta/\eta_0)]\}, \tag{22}$$

where $U_0 = U(\eta_0, \xi_0)$. According to (22), the peak should move so that

$$\xi^{pk}(\eta) = \xi^{pk}(\eta_0) + 1/3\,\eta_0 U_0 \ln(\eta/\eta_0). \tag{23}$$

Indeed, this relationship holds for $-31.6 \leqq \eta \lesssim -26.6$. In order to describe correctly the motion of the peak, an additional term $1/2\,\eta_0 U_0(1/\eta - 1/\eta_0)$ was needed for $-26.6 \leqq \eta \lesssim -11.6$. In the range $-31.6 \leqq \eta \lesssim -26.6$, allowing for a small displacement in ξ, the solution $U^{(1)}$ from (22) agrees with the numerical solution to $\sim$5%.

It is worthwhile to remark first that the early-time solution (22) predicts a constant value for the square root of the peak amplitude multiplied by the width. Indeed, this is observed in the numerical solution for all times. Secondly, a comparable amount of momentum is contained in the residue as in the pulse at the end of the run ($\eta = -6.6$). However, only a negligible portion of the energy of the initial pulse is "shared" with the residue. Finally, the main part of the solution, contained in the pulse, grows faster than $|\eta|^{-1}$ and propagates faster than a corresponding one-dimensional soliton with the same amplitude.

Numerical experiments were carried out for break-up and collision problems. The result of these problems was similar to the familiar planar results. A break-up problem is illustrated in Figure 2.

3. **Cylindrical Solitons** [3]. For the cylindrical problem, the same equations (1)–(15) hold with the exception that the divergence term $r^{-2}\,\partial/\partial r(r^2 A)$ is replaced by $r^{-1}\,\partial/\partial r(rA)$. The first order results (16)–(18) are the same. To second order, we obtain a modified *KdV* equation for the dimensionless first-order ion fluid velocity:

$$\frac{\partial U}{\partial \eta} + \frac{U}{2\eta} + U\,\frac{\partial U}{\partial \xi} + \frac{1}{2}\,\frac{\partial^3 U}{\partial \xi^3} = 0. \tag{24}$$

Note the similarity to the modified *KdV* equation for spherical solitons (19). Remember that (24) is valid for weak dispersion [$(k\lambda_D)^2 = O(\epsilon)$], weak nonlinearity [$\delta n/n_0 = O(\epsilon)$], and large radius [$r/\lambda_D = O(\epsilon^{-3/2})$].

A solution is obtained by numerically integrating (24) using an initial condition corresponding to a one-dimensional soliton

$$U(\eta_0, \xi) = 3 \operatorname{sech}^2(\xi/\sqrt{2}). \tag{21}$$

We choose η_0 such that $\xi_0 = 0$ and $\eta_0 \leqq \eta < 0$. Before discussing the numerical results, we write an approximate solution to (24) which is valid for early times $\eta \simeq \eta_0$:

$$U^{(1)}(\eta, \xi) = U_0(\eta_0/\eta)^{1/2} \operatorname{sech}\left(\left[\frac{U_0}{6}\left(\frac{\eta_0}{\eta}\right)^{1/2}\right]^{1/2} x\left[\xi - \xi_0 + \frac{2}{3}|\eta_0|^{1/2}U_0(|\eta|^{1/2} - |\eta_0|^{1/2})\right]\right), \tag{25}$$

$$\eta < 0.$$

where $U_0 = U[\eta_0, \xi^p(\eta_0)]$, and $\xi^p(\eta_0)$ is the position of the peak at $\eta = \eta_0$. By comparing this solution with the analogous solution in the spherical case, equation (22), we can draw several conclusions. First, the amplitude grows like $|\eta|^{-1/2}$ in the cylindrical case (the numerical solution grows somewhat faster than this). Second, the cylindrical soliton travels faster than the one-dimensional but slower than the spherical soliton. Finally, the width of the cylindrical soliton decreases as $|\eta|^{1/4}$ so that the square root of the amplitude, multiplied by the width, is a constant.

Using the same difference approximation method as before, (24) is integrated numerically using (21) as the initial condition. Qualitatively, the cylindrical soliton evolves in the same manner as the spherical soliton. The amplitude grows, the width decreases, and the propagation speed increases as the soliton travels inward. Figures 3(a)–(c) show the numerical solution at the initial, intermediate, and final time. A residue develops as in the spherical case. It is seen that the residue has an essentially flat distribution in ξ space as contrasted with the very broad-humped shape in the spherical problem. In the laboratory frame (r, t). the cylindrical soliton consists of a pulse moving inward radially at an ever increasing speed, greater than sound speed, leaving behind a wake.

The early time solution, given in (25), agrees with the numerical solution to better than 5% for $-31.6 \leqq \eta \lesssim -21.6$. For $\eta > -21.6$, the early time solution lags behind the numerical result. It turns out that the residue becomes nonnegligible at $\eta \sim -21.6$. Most important, the

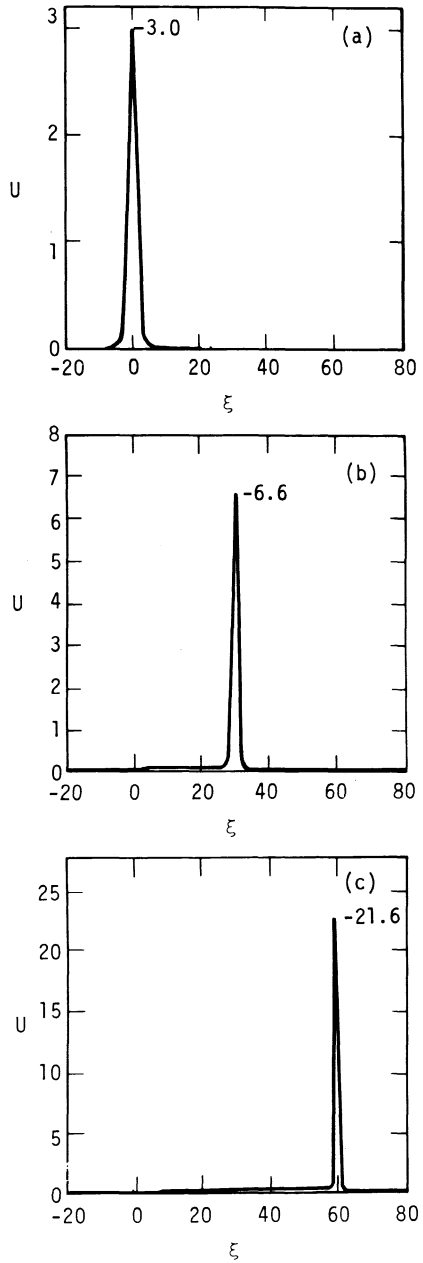

Figure 3. Evolution of cylindrical soliton. Dimensionless U versus spatial coordinate ξ at times (a) $\eta = -31.6$ (initial condition), (b) $\eta = -9.6$ and (c) $\eta = -1.6$.

square root of the peak amplitude multiplied by the width (full width at half maximum) remains constant over the entire run $-31.6 \leqq \eta \lesssim -1.6$. During this time interval, U grows by almost an order of magnitude.

4. **Comparison of Cylindrical and Spherical Solitons.** As the cylindrical soliton progresses inward, the amplitude grows somewhat faster than $|\eta|^{-1/2}$ while the width decreases somewhat faster than $|\eta|^{1/4}$. In the spherical case, the amplitude grew somewhat faster than $|\eta|^{-1}$ while the width decreased somewhat faster than $|\eta|^{1/2}$. In both the cylindrical and spherical problem the numerical solution demonstrated that the square root of the peak amplitude multiplied by the width remains constant over the entire run. This is a property of soliton solutions in one, two, and three dimensions.

Comparing the arguments of the early time solutions, we noted that the cylindrical soliton travels slower than the spherical but faster than its planar counterpart with the same amplitude.

As remarked earlier, the residue in the cylindrical problem has a much flatter distribution in ξ than in the spherical problem. In order to compare the magnitude of the residue in the two problems, consider the first conserved quantity corresponding to (24).

$$Q_1^{(c)} = |\eta|^{1/2} \int_{-\infty}^{\infty} d\xi\, U. \tag{26}$$

The analogous quantity in the spherical case, (19), is

$$Q_1^{(s)} = \eta \int_{-\infty}^{\infty} d\xi\, U. \tag{27}$$

Denote the integrals over the residue by $q_1^{(c)}$, $q_1^{(s)}$.

In Table I, we compare $q_1^{(c)}/Q_1^{(c)}$ and $q_1^{(s)}/Q_1^{(s)}$ at times $\eta^{(c)}$, $\eta^{(s)}$ such that the peak velocity, U^p, is comparable. The superscript c refers to the cylindrical problem while s refers to the spherical problem. The results show that the residue in the two problems contributes an almost identical percentage of the conserved quantity Q_1, except at the earliest time.

TABLE 1: Contribution of Residue in Cylindrical and Spherical Problems

$\eta^{(c)}$	U^p	$q_1^{(c)}/Q_1^{(c)}$	$\eta^{(s)}$	U^p	$q_1^{(s)}/Q_1^{(s)}$
−26.6	3.34	.017	−28.6	3.38	.011
−21.6	3.83	.05	−25.6	3.92	.05
−11.6	5.79	.14	−19.6	5.60	.13
− 6.6	8.43	.22	−14.6	8.30	.22
− 2.6	15.65	.33	− 9.6	14.53	.32

5. **Experimental Observation of Cylindrical Solitons.** The observation of cylindrical solitons was carried out by Noah Hershkowitz of the University of Iowa and reported in [4]. This section is taken from his work.

Experiments were carried out using the University of Iowa cylindrical double plasma device shown in Figure 4. Two concentric cylindrical plasmas (length 30 cm) are separated by two closely spaced, fine-mesh, concentric cylindrical screens with inner screen diameter equal to 20 cm. The outer screen is negatively biased to prevent the flow of electrons between the plasmas, and the inner screen is grounded. The ion density was approximately 10^9 cm^{-3} and the ion and electron temperatures were approximately 0.2 and 3 eV, respectively. Positive half-sine-wave pulses are applied to the outer plasma to launch cylindrical density perturbations in the inner plasma.

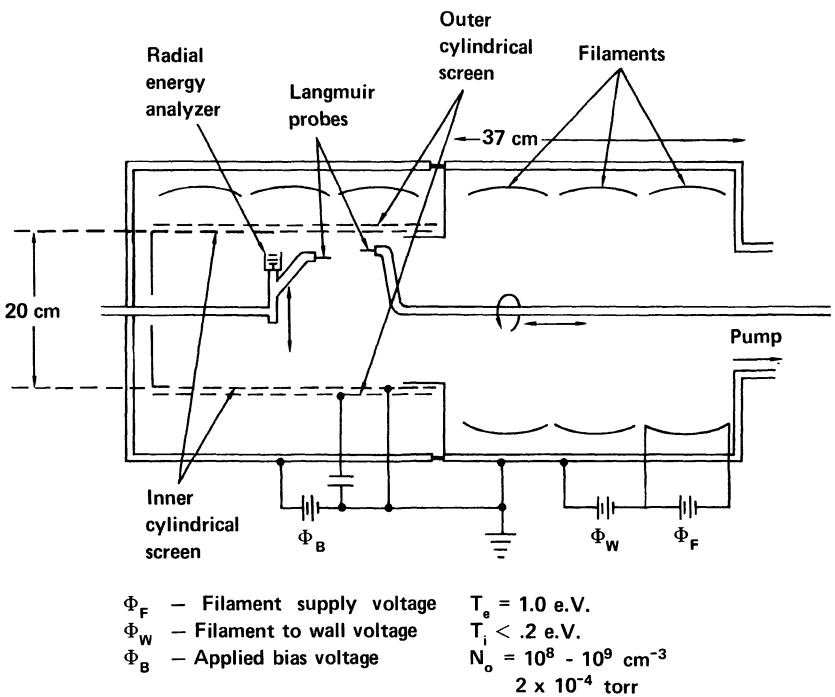

Figure 4. University of Iowa Cylindrical Double Plasma Device [by permission of N. Hershkowitz].

Signals are detected by a positively biased Langmuir probe which has variable radial position. No azimuthal dependence was observed. Figure 5(a) shows the perturbed electron number density as a function of time at several radial positions for both large and small initial density perturbations. For the small-amplitude pulse at $r = 9$ cm we can identify an ingoing pulse, which is quite similar to the applied pulse, followed at a later time by the similar outgoing pulse that has propagated from the opposite side and through the center. As the probe is moved closer to the center, the ingoing and outgoing pulses approach each other, merging at the center. For the large-amplitude compressive pulse at $r = 9$ cm the ingoing pulse is seen to be similar to the applied pulse, but three solitons can be identified in the outgoing pulse. The traces at other radial positions indicate how the initial density perturbation evolves into the solitons. The increased velocity of the first two solitons compared to the ion acoustic velocity is evident. Once formed, the largest soliton is seen to be much narrower than the applied pulse. We find that the average velocity of the largest ingoing soliton is approximately $1.17c_s$. The application of a negative (rarefactive) density perturbation is not found to evolve into solitons.

As in the one-dimensional DP device, the maximum applied voltage is limited by the electron temperature. For applied voltages larger than the electron temperature ($\sim 3\,eV$), particle bursts (pseudowaves) are detected. Data were taken with the largest initial density perturbation that could be obtained without launching pseudowaves. The width of the applied pulse was then varied to determine how the soliton number depended on the initial density perturbation (see Fig. 5). Figure 5b) shows how the signal received, $r = 0.5$ cm, depends on applied pulse width. Widening the applied pulse results in increased amplitude, decreased width, and increased velocity in the received signal. In the top trace we see one well-defined soliton. In the second trace, the first soliton has grown and narrowed and a second soliton is apparent. In the third trace the first two solitons have grown, narrowed, and speeded up. A third soliton is barely apparent. We find that the square root of the maximum amplitude multiplied by the width is constant to within 10% for the first four traces. In the fourth trace the third soliton is seen to grow as well. For further increases in width, the solitons no longer have sufficent time to separate from the initial perturbation. Figure 5(c) shows the signals corresponding to the same six applied pulse widths as detected at $r = 6$ cm.

This experiment differs from an idealized one in at least two respects. First, as in one-dimensional experiments, damping is present. Second, the density perturbation is not found to diverge at the center.

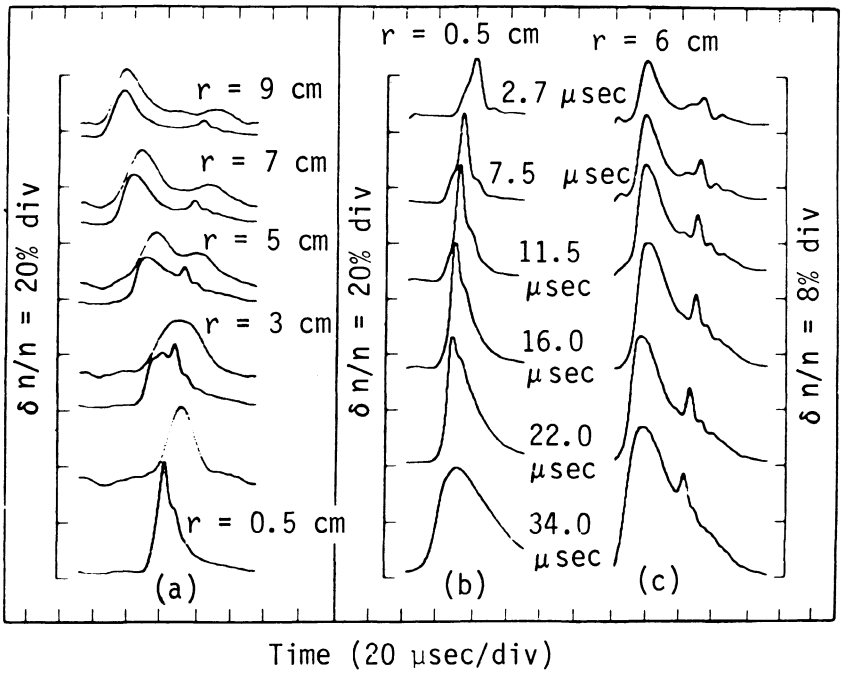

Figure 5. (a) Perturbed electron number density as a function of time at several radial positions. Upper traces, linear ($\delta n/n < 1\%$) ion acoustic pulses (with amplitude adjusted for comparison). Lower traces, nonlinear pulses propagating, steepening, and breaking into solitons. (b) Perturbed electron number density detected at $r = 0.5$ cm labeled by the applied pulse widths. (c) Received signals at $r = 6$ cm labeled by applied pulse width [from Ref. 4 by permission of N. Hershkowitz].

We attribute this result in part to broadening of the received pulse as a result of variations in the radius of the cylindrical screens of the order of 0.3 cm and to finite size of the probe and of an insulating glass cylinder (0.5 cm) which covers all but the last centimeter of the probe.

6. **Summary and Discussion.** The basic difference between the one-dimensional soliton and its counterpart in two and three dimensions is the absence of a residue, or wake. The basic similarity is the constant value of the square root of the amplitude multiplied by the width in one, two, and three dimensions. Whereas the amplitude is a constant in one dimension, it increases faster than $|\eta|^{-1/2}$ in the cylindrical case and $|\eta|^{-1}$ in the spherical case. The residue in the cylindrical case is rather flat in ξ space whereas the shape is a very broad hump in the spherical case. In both the cylindrical and spherical problems, the residue con-

tributes an almost identical percentage of the first conserved quantity when the amplitudes of the two solitons are comparable.

Break-up of initial disturbances into N solitons and oscillatory tails has been observed in cylindrical and spherical geometry, yielding results similar to the one-dimensional case. Also, the nonlinear interaction of two solitons in one dimension, which preserves their shape and speed, is seen here for both the cylindrical and spherical solitons.

7. **Unresolved Problems.** Perhaps the most immediate challenge is to apply the inverse method or the method using the conservation laws to the initial value problem for (19) and (24). However, the mathematical problem with the greatest significance, in the opinion of the author, is the discovery of a solution to a modified KdV equation (planar, cylindrical, or spherical) with a damping term comparable in size with the nonlinear and dispersive terms. Such equations have been derived in the literature and take the form [5] (for planar wave front)

$$\frac{\partial U}{\partial \eta} + U\frac{\partial U}{\partial \xi} + \frac{1}{2}\frac{\partial^3 U}{\partial \xi^3} + \frac{1}{\sqrt{8\pi}}\int_{-\infty}^{\infty}\frac{d\xi'}{(\xi - \xi')}\frac{\partial U}{\partial \xi'} = 0 \tag{28}$$

with the principal value integral term giving the contribution from Landau damping.

The importance of finding solutions with stong damping lies in possible applications of soliton work to fusion. After propagating waves a distance into the plasma, we want to arrange the physical parameters (density, temperature, magnetic field, etc.) so that the waves will dissipate, thereby heating the plasma particles. This process of energy exchange between waves and particles can only be understood when we know how to describe wave motion with strong damping.

References

1. A. C. Scott, F. Y. F. Chu, and D. W. McLaughlin, *The soliton: A new concept in applied science*, Proc. IEEE **61** (1973), 1443–1483.

2. S. Maxon and J. Viecelli, *Spherical solitons*, Phys. Rev. Lett. **32** (1974), 4–6, and references therein.

3. ———, *Cylindrical solitons*, Phys. Fluids **17** (1974), 1614–1616.

4. N. Hershkowitz and T. Romesser, *Observations of ion-acoustic cylindrical solitons*, Phys. Rev. Lett. **32** (1974), 581–583.

5. T. Taniuti, *Ion-acoustic solitary waves with effects of resonant particles*, Prog. Theor. Phys. Suppl. **55** (1974), 191–211.

Lawrence Livermore Laboratory, University of California, Livermore, California 94550